Injectable shear thinning hydrogels for delivering osteogenic and angiogenic cells and growth factors

Emine Alarçin[†,a,b,c], **Tae Yong Lee**[†,a,b,d], **Sobha Karuthedom**[a,b], **Marzieh Mohammadi**[a,b], **Meadhbh A Brennan**[a,b,e], **Dong Hoon Lee**[a,b], **Alessandra Marrella**[a,b], **Jin Zhang**[a,b], **Denata Syla**[a,b], **Yu Shrike Zhang**[a,b,f], **Ali Khademhosseini**[a,b,f,g,h,i,j,k,l], and **Hae Lin Jang**[a,b,f]

[a]Division of Engineering in Medicine, Department of Medicine, Harvard Medical School, Brigham & Women's Hospital, Cambridge, MA 02139, USA

[b]Division of Health Sciences & Technology, Harvard-Massachusetts Institute of Technology, Massachusetts Institute of Technology, Cambridge, MA 02139, USA

[c]Department of Pharmaceutical Technology, Faculty of Pharmacy, Marmara University, Istanbul 34668, Turkey

[d]Department of Chemical and Biomolecular Engineering, Korea Advanced Institute of Science and Technology (KAIST), Daejeon 34141, South Korea

[e]INSERM, UMR 1238, PHYOS, Faculty of Medicine, University of Nantes, Nantes, France

[f]Wyss Institute for Biologically Inspired Engineering, Harvard University, Boston, MA 02115, USA

[g]Department of Bioindustrial Technologies, College of Animal Bioscience & Technology, Konkuk University, Seoul 143-701, Republic of Korea

[h]Center of Nanotechnology, Department of Physics, King Abdulaziz University, Jeddah 21569, Saudi Arabia

[i]Department of Bioengineering, Department of Chemical and Biomolecular Engineering, Henry Samueli School of Engineering and Applied Sciences, University of California-Los Angeles, Los Angeles, CA, USA

[j]Department of Radiology, David Geffen School of Medicine, University of California-Los Angeles, Los Angeles, CA, USA

[k]Center for Minimally Invasive Therapeutics (C-MIT), University of California-Los Angeles, Los Angeles, CA, USA

[l]California NanoSystems Institute (CNSI), University of California-Los Angeles, Los Angeles, CA, USA

Abstract

Correspondence to: Yu Shrike Zhang; Ali Khademhosseini; Hae Lin Jang.

[†]These authors contributed equally to this work.

Bone nonunion may occur when the fracture is unstable, or blood supply is impeded. To provide an effective treatment for healing of nonunion defects, we introduce an injectable osteogenic hydrogel that can deliver cells and vasculogenic growth factors. We used a silicate-based shear-thinning hydrogel (STH) to engineer an injectable scaffold and incorporated polycaprolactone (PCL) nanoparticles that entrap and release vasculogenic growth factors in a controlled manner. By adjusting the solid composition of gelatin and silicate nanoplatelets in the STH, we defined optimal conditions that enable injection of STHs, which can deliver cells and growth factors. Different types of STHs could be simultaneously injected into 3D constructs through a single head composed of multiple syringes and needles, while maintaining its engineered structure in a continuous manner. Injected STHs were also capable of filling any irregularly shaped defects in bone. Osteogenic cells and endothelial cells were encapsulated in STHs with and without vasculogenic growth factors respectively, and when co-cultured, their growth and differentiation were significantly enhanced compared to cells grown in monoculture. This study introduces an initial step of developing a new platform of shape tunable material with controlled release of angiogenic growth factors by utilizing PCL nanoparticles.

1. Introduction

Approximately one in three people experience a bone fracture during their lifetime, and up to 10% of these bone fractures are associated with impaired healing.[1–4] Nonunion is a permanent failure of a broken bone to heal, which can occur when the fracture is unstable or has serious interruptions in blood supply.[1,5] Since blood delivers oxygen, nutrients, and cells to bone, impaired blood supply at the bone defect can delay bone healing or even cause a destruction of bone tissue.[6–9] Nonunion fractures cause severe pain, infection, and disability, and hence further surgical intervention and clinical treatments are necessary. Autologous transplantation is considered the gold-standard for bone defect repair due to its histocompatibility and non-immunogenicity.[10] Autologous bone grafts have a vascularized structure and thus can easily achieve revascularization and anastomose with the surrounding tissues.[9] However, there is a limited quantity of available bone tissues to harvest and there is associated donor site morbidity.[11–13] Another approach for treating nonunion is allografting, but this has an increased risk of disease transmission, infection, and immune response.[14] To replace autologous or allogenic bone grafts, various types of artificial bone implants have been developed and used in the clinic. However, despite recent advances in orthopedics research, most current bone implant materials are restricted to the inorganic bone materials, and vascularized synthetic bone grafts have not yet been utilized in the clinic, resulting in a lower success rate compared with autologous bone grafting.[15] Sintered calcium phosphate ceramic bone implants are also difficult to fill irregularly shaped bone defects or used for minimally invasive treatment.[16] Although polymethyl methacrylate (PMMA) cement or calcium phosphate cement can fill an irregular shaped bone defect site, it is difficult to deliver vasculogenic growth factors and cells for vascularization, because of the high-density nature of bone cement and exothermic reactions that often occur during the curing process.[17,18]

Bone is a highly vascularized tissue, where osteogenesis and vascularization are coupled, and synergistic cross-talks between bone cells and vascular cells exist during bone

regeneration.[9,19–21] When mesenchymal stem cells (MSCs) and endothelial cells are co-cultured, both osteogenic and angiogenic markers are enhanced compared to cells cultured in monoculture, leading to enhanced mineralization.[22–25] On the other hand, damage to bone vasculature can inhibit bone growth and induce skeletal diseases.[26–29] In the context of bone regeneration using synthetic biomaterial constructs, an insufficient formation of a blood vessel network can impair bone healing or even cause tissue necrosis. However, until now, the development of a vascularized bone implant remains a challenge due to the difficulty of simultaneously regulating multiple tissue types of bone and blood vessels that have distinct physicochemical properties such as stiffness, and growth factors. Moreover, developing a continuous junction between highly vascularized bone grafts and the surrounding tissues is complex, because of the heterogeneity of the size and shape of bone fractures.

In this preliminary study we designed and engineered injectable hydrogels with osteogenic and vasculogenic components to overcome critical barriers to developing a shape-tunable vascularized bone implant (Fig. 1). We utilized silicate nanoplatelets (Laponite: ($Na^+_{0.7}[(Mg_{5.5}Li_{0.3})Si_8O_{20}(OH)_4]^-_{0.7}$)) and gelatin to develop an osteogenic shear-thinning hydrogel (STH), which can flow when the minimum shear force is applied and rapidly gel after injection into a cavity. Silicate materials can intrinsically induce osteogenic differentiation of human MSCs.[30] In addition, silicate nanoplatelets have an anisotropic distribution of surface charge, where the charge of the edge of the platelets is positive, and the charge of the flat top and bottom surfaces is negative.[31] Based on this unique anisotropic charge distribution, silicate nanoplatelets can form an STH structure in aqueous media, which can dynamically integrate and break. Gelatin contains positive and negative regions that can form strong cross-linked networks with the oppositely charged surface of silicate nanoplatelets through electrostatic interactions.[32–36] Silicate and gelatin-based STHs have been previously applied for the treatment of hemorrhage and endovascular embolization. [37,38] Notably, here, we further incorporated biodegradable polycaprolactone (PCL) nanoparticles into the STH as drug carriers to achieve entrapment and controlled release of vasculogenic growth factors over time, to direct vascular differentiation of endothelial cells. In particular, we selected vascular endothelial growth factor (VEGF) since it plays a crucial role in angiogenesis and bone formation.[39,40] Besides, PCL nanoparticles exhibit negative electrostatic charges similar to silicate nanoplatelets.[41] Therefore, the negatively charged PCL nanoparticles can also interact with the positively charged gelatin and maintain the shear-thinning property of STH.

This study was the first step in the development of a novel injectable cell-laden implant incorporating an osteogenic hydrogel coupled with a hydrogel with controlled release of VEGF to potentially enhance bone formation. The mechanical characteristics of the biomaterials were optimized to achieve the shear-thinning property. We then showed a synergistic effect between the osteogenic STHs and VEGF-releasing STHs for enhancing cellular proliferation and differentiation. We further used a novel, customized multi-material injecting device with a single head through which multiple materials could be simultaneously injected for *in situ* gelation. We finally demonstrated the ability of our injectable materials to fill cavities of varied geometries and *ex vivo* bone defects.

2. Materials and Methods

2.1. Fabrication of PCL nanoparticles

PCL nanoparticles were prepared by the previously described water-in-oil-in-water (W_1/O/W_2) double emulsion solvent evaporation method with slight modifications.[42] PCL with the number of average molecular weight (Mn) 80000 was used (Sigma Aldrich, St. Louis, USA) for nanoparticle fabrication. Either fluorescein isothiocyanate (FITC)-dextran molecules (40 kDa, Sigma Aldrich, St. Louis, USA) or VEGF (Recombinant human VEGF 121, 28.4 kPa, Peprotech, USA) with bovine serum albumin (BSA, Sigma Aldrich), was encapsulated within the PCL nanoparticles. FITC-dextran was chosen as it can simulate the release behavior of growth factors, based on their similar range of molecular weights and hydrophilic behavior. BSA was mixed at the W/O interface to form a protective shell around VEGF and preserve their bioactivity as well as enhancing the encapsulation efficiency.[43,44] First, we prepared stock solutions of 2% and 0.1% polyvinyl alcohol (PVA, Sigma Aldrich) by mixing PVA with deionized (DI) water and stirred overnight at 40 °C. Then 10 mL of 2% (w/v) PVA aqueous solution containing 25 mg BSA and either 10 mg FITC-Dextran, or VEGF (10 µg) was emulsified in an oil phase solution of 250 mg of PCL dissolved in 5 mL of dichloromethane (DCM, Sigma Aldrich) by using a probe-type ultrasonic homogenizer (Qsonica Sonicator, #Q500, Newton, CT, USA) with various amplitude and exposure time (Table 1). This primary emulsion was re-emulsified in 30 mL of 0.1% (w/v) PVA solution using an ultrasonic homogenizer with various amplitudes and exposure times (Table 1) and then stirred for 2 h using a magnetic stirrer to evaporate the organic solvent completely. PVA can stabilize both W/O and O/W interfaces, and therefore W/O/W double emulsion drops can be fabricated by the two-step emulsification method described. The obtained nanoparticles were collected by centrifugation at 13500 rpm for 10 min, and washed three times with DI water. To study the influence of different particle sizes on VEGF release, we produced nanoparticles with various sizes by controlling the ultrasonication amplitude and exposure time during the emulsification. The particles were prepared at the ultrasound amplitude conditions of 50%, 40%, and 30% and exposure times were 5 min, 3 min, and 1 min, respectively.

2.2. Characterization of PCL nanoparticles

2.2.1. Size and morphological characterization of PCL nanoparticles—The size and morphology of lyophilized PCL nanoparticles were evaluated by a field emission scanning electron microscope (FESEM, Ultra 55, Zeiss). Samples were gold-coated with a 10 nm thickness layer and observed at an acceleration voltage of 10 kV. The mean particle diameter, and zeta potential of nanoparticles were determined by dynamic light scattering (DLS, Malvern Zetasizer Nano ZS, UK).

2.2.2. Release profile from PCL nanoparticles—FITC-dextran release studies were carried out by incubating PCL nanoparticles in phosphate buffered saline (PBS, pH 7.4) at 37 °C with constant agitation. At predetermined time intervals, the tubes were centrifuged and 100 µl supernatant was collected for analysis and returned after measurement. The supernatant was analyzed for FITC-dextran content by measuring fluorescence intensity with excitation and emission wavelengths at 490 and 520 nm using microplate reader

(Synergy 2, HT-Reader, BioTek, Winooski), respectively. Each formulation was studied in triplicate.

2.3. Fabrication of STH with PCL nanoparticles

STH was prepared according to a previously described method.[37,38] Briefly, the stock solution of 18% (w/v) gelatin was prepared by dissolving 1.8 g gelatin (G1890, Sigma-Aldrich) in 10 mL DI water at 80 °C for 20 min. The 9% (w/v) nanosilicate (Laponite XLG, BYK) stock solutions (0.09 g/ml) was prepared by vortexing nanosilicate in DI water at 4 °C to obtain a clear gel. Subsequently, stock solutions of gelatin and nanosilicate were mixed by 1:2 (wt%) with additional DI water for 5 min to generate STHs with the desired concentration (6 or 7 total solid weight percent and notating as 6STH or 7STH). STH was mixed with PCL nanoparticles at room temperature. PCL nanoparticle concentration was consistently 1.25 mg per mL STH gels. To visualize the homogeneous dispersion of the PCL nanoparticles within the STH, fluorescent images of FITC-dextran loaded PCL nanoparticles within the STH were acquired by using a fluorescent microscope (Zeiss, Axio observer D1). For easier visualization of particles in STH, for only this experiment, we increased the concentration of PCL in STH to 20 mg/mL.

2.4. Characterization of STH with PCL nanoparticles

2.4.1. Injectability of STH with PCL nanoparticles—The injectability of the material was analyzed using a mechanical tester (Instron Model 5542).[37] Briefly, the STH was added to 3 mL plastic syringes (inner diameter: 8.66 mm; BD Biosciences) and injected through needles (18 gauge, BD Biosciences). The injection rate was controlled by changing the cross speed of the compression plate to achieve the desired flow rates. Each measurement was performed in triplicate.

2.4.2. Degradation of STH with PCL nanoparticles—The degradation rate of 6 and 7 wt% STH containing PCL nanoparticles was monitored at 37 °C over 50 days under constant agitation. Briefly, 0.5 g of STH including PCL nanoparticles was added to a (1.5 mL) solution in an Eppendorf tube. At each time point, swollen STH with PCL nanoparticles were weighed after centrifuging the sample at 1000 rpm for 5 min and carefully removing the excessive amount of media that remained on the surface of the hydrogel using a filter paper. After the measurement, media was added back onto the STH with PCL nanoparticles for further degradation assessment. The percentage of the remaining mass of the nanocomposites was calculated by weighing STH at different time points. All of the experiments were carried out in triplicate.

2.5. Rheological Analysis

Rheological properties were characterized using a rheometer (TA instruments, ARES-G2, DE, USA) equipped with a 20 mm diameter parallel plate geometry and a gap of 500 μm. All tests were conducted at 37 °C. To avoid evaporation of water, mineral oil was cast around the circumference of the plate. Strain sweeps were conducted from 0.1 % to 1000 % strain at 1 Hz. Recovery testing was performed at 1 Hz and 37 °C by applying 1 % strain for 5 min, followed by applying 100 % strain for 5 min as a value out of the linear viscoelastic range, for 4 cycle to monitor gel recovery. Each analysis was carried out in triplicate.

2.6. STH with PCL nanoparticles to fill voids and defects of varied geometries

2.6.1. Injection of STH into varied shapes—To determine whether STH can be injected into voids of varied shapes, transparent polydimethylsiloxane (PDMS) molds of distinct geometries were prepared. The 6STH and 7STH including PCL nanoparticles were prepared as described earlier and mixed with colored dyes. They were loaded into syringes (5 mL) with needles (18 gauge), after which they were injected into the PDMS molds. Photographs were taken to document the filling of the mold by the STHs.

2.6.2. Injection of biomaterial gel into *ex vivo* porcine femur defects—After testing the gel in a PDMS mold, an *ex vivo* experiment was performed to test the injectability of the STH into real bone tissue to mimic a bone defect. A porcine femur bone was acquired and defects were created by drilling cavities in the bone. Defects of small size and large size were made for comparison. The 6STH and 7STH including PCL nanoparticles were prepared as described earlier and mixed with colored dyes. They were loaded into syringes (5 mL) with needles (18 gauge), after which they were injected into the created defect sites. Photographs were taken to document the filling of the cavity by the STHs.

2.7. 3D Injection of STH

To 3D inject the STH scaffolds, a customized multi-material injecting device was used [45]. Two different concentrations of STH; 6STH and 7STH comprising PCL nanoparticles were loaded into separate syringes. To better visualize the injection of distinct materials and scaffold interfaces, colored dyes were added to the each STH. Each syringe had an 18 gauge needle attached at their outlets and were merged into one outlet using a custom design. The reservoirs were connected to the pneumatic pump to apply pressure to inject the STH.

2.8. *In vitro* assessment of cell-laden STH with PCL nanoparticles

To evaluate the biocompatibility of the STH containing PCL nanoparticles, we used mouse endothelial cells and osteoblasts. Mouse primary mammary microvascular endothelial cells (BALB/c, BALB-5020, Cell Biologics) were expanded in endothelial cell medium with a supplement kit (Cat No M1168, Cell Biologics). Mouse osteoblasts (CRL-12557, ATCC) were expanded in Dulbecco's modified Eagle medium (DMEM, Gibco) supplemented with 10% fetal bovine serum and 1% penicillin/streptomycin. Cells were cultured in 5% CO_2 humidified incubators at 37 °C with media changes 3 times per week. Cells of passage 5–7 were used for experiments.

Endothelial cells were seeded in 6STH gels containing PCL nanoparticles (with or without VEGF) and osteoblasts were seeded in 7STH gel, both at a density of either 2 or 5×10^6 cells/mL gel according to experiment. For groups where both endothelial and osteogenic gel portions were injected, a cell ratio of 1:1 was used. The cell-laden gels were injected through syringes with 18 gauge needles. The gel with encapsulated cells was injected into the wells of a 48 well plate (200 μl scaffold per well) covered with 500 μL culture medium (ratio of 1:1 culture media for co-culture set-ups). Cell-laden STH gels with PCL nanoparticles were cultured for either 7 or 21 days and assessed for cell viability and proliferation.

2.8.1. Live/dead staining—The Live/Dead assay was performed to assess cell viability according to the manufacturer's instructions (ThermoFisher Scientific) at days 1, 3, and 7. An initial cell plating density of 2×10^6 cells/mL of gel was used and gels were without PCL nanoparticles. Briefly, the cells were stained with calcein AM (green) for live cells and ethidium homodimer-1 (red) for dead cells in PBS. The stained cells were imaged using an inverted fluorescent microscope (Zeiss Axio observer D1, NY, USA). The numbers of live and dead cells were calculated by analyzing the acquired six images from three different nanocomposite samples for each condition using NIH Image J Software.

2.8.2. Cell proliferation analysis—A PrestoBlue® Cell Viability Reagent was used to evaluate cell metabolic activity according to the manufacturer's instructions at days 1, 3, and 7. An initial cell plating density of 5×10^6 cells/mL of gel was used and gels were with or without VEGF-loaded PCL nanoparticles. At each time point, samples were rinsed with PBS after removing the media. Briefly, 500 μL of PrestoBlue solution, which was prepared at a concentration of 1:10 with cell culture media, was added to each well and the samples were incubated at 37 °C. Subsequently, 100 μl of the solution was transferred to wells of a 96-well plate and absorbance was read at an excitation of 530 nm and emission of 590 nm using a plate reader (Synergy 2, HT-Reader, BioTek, Winooski). For each condition, the samples were tested in triplicates.

2.8.3. Live cell tracker analysis—Since both live/dead and presto blue assessments did not differentiate between the osteoblast and endothelial cell types, we performed live cell tracking to identify each of the respective cell types over time. Osteoblast were labeled with green CMFDA cell tracker (C2925, Molecular Probes, Invitrogen) and endothelial cells were labeled with red CMTPX cell tracker (C34552, Molecular Probes) according to the manufacturer's protocol. Both cell types were incubated separately in 10 mM dye solution in serum-free DMEM for 30 min at 37 °C in 5% CO_2 humidified incubators, followed by several washes in PBS to remove the unbound dye solution. An initial cell plating density of 2×10^6 cells/mL of PCL nanoparticle-laden gel was used. Cell-laden gel constructs were observed under a florescent microscope on days 1, 3, 7, and 21 of culture.

2.9. *In vitro* assessment of cell-laden STH with VEGF-encapsulated PCL nanoparticles

Once biocompatibility of PCL nanoparticles within the STH was established, we then sought to investigate the capability of growth factor encapsulated PCL nanoparticles to promote cellular differentiation. In particular, we employed VEGF to enhance vasculogenic activity of cells. Poietics™ Normal Human Bone Marrow Derived Mesenchymal Stem Cells (BMSC, Lonza PT-2501), and Human Umbilical Vein Endothelial Cells (HUEVC, Lonza), were expanded in DMEM supplemented with fetal bovine serum (FBS, 10% v/v) and complete endothelial cell growth medium (EGM2 media, Lonza). BMSCs (2×10^5 cells), HUVEC (2×10^5 cells), or co-cultures of both cell lines were encapsulated in 200 μL of STH containing 40 mg of VEGF-encapsulated particles and were cultured in DMEM supplemented with FBS (10% v/v) for 7 days.

2.9.1 RNA isolation and real time polymerase chain reaction (RT-PCR) analysis —After 7 days of culture, samples were washed with PBS and treated with 1 mL of Trizol

reagent (Life Technologies). Subsequently, the total extracted RNA underwent reverse transcription to cDNA using a reverse transcriptase kit (Qiagen) in a programmable thermal cycler (PTC-100). The expression of osteogenesis related genes such as alkaline phosphatase (*ALP*), osteopontin (*OPN*), osteocalcin (*OCN*), and angiogenesis-related genes such as vascular cell adhesion molecule (*VCAM*) and von willebrand factor (*VWF*) were evaluated using RT-PCR. Primer sequences are shown in Table 2. Quantitative RT-PCR was performed using a SYBR Green PCR super mix kit (BioRad, USA) on a RT-PCR system (Bio-Rad iQ5 Multicolor Real-Time PCR Detection System). Thereafter, relative gene expression was analyzed using $2^{-(\Delta\Delta Ct)}$ method and glyceraldehyde 3-phosphate dehydrogenase (*GAPDH*) was chosen as the endogenous housekeeping gene.

2.10. Statistical analysis

Results were presented as means ± standard deviations (n=3). One-way analysis of variance (ANOVA) was conducted for analysis of VEGF release from PCL nanoparticles. For PrestoBlue analysis a 2-way ANOVA was used with Tukey's multiple comparison. For gene expression results an unpaired 2 sample T-test was employed for statistical analysis. Threshold for statistical significance for all tests was at $p<0.05$.

3. Results and discussion

3.1. Fabrication and Characterization of PCL nanoparticles

We first utilized a W/O/W emulsification method to prepare PCL nanoparticles to form a matrix type structure to achieve sustained release of VEGF. To determine an optimized size of particles for delivering growth factors, as shown in Table 1, we controlled the experimental conditions during the W/O/W double emulsion process with three formulation codes (SNP for preparing small-sized nanoparticles, MNP for preparing medium-sized nanoparticles, and LNP for preparing large-sized nanoparticles). In particular, we decreased the amplitude and duration of the ultrasonication process from SNP to LNP to regulate the size of the PCL particles. The increasing intensity and longer application of ultrasonication increases the effect of shear stress and the energy applied, causing the reduction of droplet size, leading to a decrease in particle size.[46,47] As shown in Fig. 2a, from the FESEM images, we can observe that the obtained particles were spherical in shape with a smooth surface morphology and the size of the synthesized PCL nanoparticles had significantly changed according to the different formulations. From the DLS analysis, the average sizes of the PCL nanoparticles generated from SNP, MNP, and LNP formulations were measured to be 268±11 nm, 429±17 nm, 743±37 nm, respectively, which corresponded well with the sizes of particles observed in the FESEM images. Additionally, the zeta potential values of PCL particles prepared by SNP, MNP and LNP formulations were −22.40 mV, −21.83 mV, −22.6 mV respectively, which resulted in highly stabilized PCL nanoparticles without particle aggregation based on electrostatic repulsion.[41,48] STH has shear thinning behavior due to electrostatic interactions between negatively charged silicate nanoplatelets and positively charged gelatin.[38] Hence, negatively charged PCL nanoparticles can also interact with gelatin to maintain the shear thinning behavior.

To examine the capacity of PCL nanoparticles to entrap and release biomolecules, we utilized the FITC-dextran molecules that can simulate the release behavior of VEGF based on its similar range of molecular weight and ease of quantitative detection based on its fluorescence level. We encapsulated FITC-dextran molecules in the solid matrix of the PCL nanoparticles. We then measured the release profile of the fluorescent molecules from the PCL nanoparticles-incubated in PBS solution over time by measuring the fluorescence intensity level of the supernatant of the system.

As shown in Fig. 2b, the release profiles of all three groups of the differently sized PCL nanoparticles had a biphasic release pattern with an initial burst phase, followed by a sustained release, which is in agreement with previous literature.[49–51] This biphasic release profile of the fluorescent molecules from the PCL nanoparticles fitted well with exponential decay equation model, $c(t) = (1 - exp^{-\frac{t}{\tau}})$, where c(t) is the cumulative release of the molecules at specific time t, and τ stands for the time constant for burst release.[52] The initial burst release attributed to early release of molecules that are weekly bound to the surface of the particles.[49] The time period to achieve 50% release of FITC-dextran molecules in differently sized nanoparticles increased as the size of the particles became larger (SNP: 6.0 hours, MNP: 16.3 hours, LNP: 37.0 hours) because the higher surface area of the smaller nanoparticles resulted in higher drug amount on the nanoparticle surface. The characteristic timescale for the burst release (τ) also increased as the size of the nanoparticles became larger (SNP: 8.4 hours, MNP: 24.0 hours, LNP: 52.8 hours). PCL nanoparticles prepared by the LNP formulation took more than 2 days to release 63% of encapsulated molecules while releasing the same amount of encapsulates took only about 8 hours for PCL nanoparticles prepared by the SNP formulation. This initial burst release was useful for our designed system to achieve early vascularization, which is critical for bone regeneration.[53,54] Burst release was followed by sustained release of the remaining molecules over 7 days for all the formulations. This sustained release can be mainly caused by the slow degradation rate of polymers and hence release of molecules from nanoparticles is a consequence of biomolecule diffusion and matrix erosion.[51, 55] We also monitored if FITC-dextran encapsulated PCL nanoparticles could homogeneously disperse in silicate- and gelatin-based STH because uneven distribution of PCL nanoparticles can affect injectability of the composite material and injection quality. After sufficient vortexing of PCL nanoparticles in STH that had a composition of 20 mg/mL (2%), FITC-dextran-loaded PCL nanoparticles were found to disperse homogeneously in the hydrogel matrix and were visualized under a fluorescent microscope, as shown in Fig. 2c.

3.2. Fabrication and characterization of STH with PCL nanoparticles

We then fabricated various formulations of STHs with and without incorporation of PCL nanoparticles. STHs were fabricated without PCL nanoparticles at first. Herein, the total solid weight percent in the STH hydrogel (silicate nanoplatelets + gelatin), x wt%, 3<x<9) and the weight percent of silicate nanoplatelets in total solid content (y wt%, 25<y<75) were labeled as xSTHy. After changing the weight percent of silicate nanoplatelets and gelatin (xSTHy) in STH to define optimal composition to achieve the shear-thinning property and enable its injection, PCL nanoparticles were incorporated into STHs labeled as xSTHy-PCL.

PCL amount was kept consistent for all formulations as 1.25 mg PCL nanoparticles per 1 mL STH.

The injectability of various formulations of STHs with and without PCL nanoparticles was then examined. When the total solid weight percent of silicate nanoplatelets and gelatin (x wt%) was lower than 5 wt%, STH behaved like a liquid and easily deformed once it was injected by our customized injecting device. Conversely, when the total solid weight percent of silicate nanoplatelets and gelatin was above 8 wt%, STH became too viscous and required high pressure to be injected, often leading to the leakage of the reservoirs. In this respect, we concluded that STHs with the total solid content in the range of 6–7 wt% was optimal for the injection. Similarly, it was difficult to inject when the weight percent of nanoplatelets was high, such as in the case of 7STH75. Since silicate nanoplatelets have an osteogenic function, we thus used 50 wt% of silicate nanoplatelets in the total solid content.

To quantitatively examine the injectability of PCL-incorporating STHs with different nanoparticle sizes, we conducted the injection force measurement by using an Instron mechanical tester. When the injection flow was applied to STHs at a constant rate of 2 mL/min, the injection force linearly increased to the maximum point, which then slightly decreased and finally maintained a plateau phase. The frictional force between the surface of the syringe and STHs and the internal network structure of STHs before the extrusion of STHs from the syringe may have caused the initial increase of the injection force. As the shear stress applied to STHs gradually increased, the internal structure of STH became more disturbed and its viscosity decreased, resulting in a decreased injection force, and inducing the final force to reach plateau values (Fig. 3a). We used the maximum value at the plateau phase to quantify the injection force. As shown in Fig. 3b, we confirmed that it required a minimum level of force to inject 6STH50 (1.10±0.22 N) and 7STH50 (1.66±0.16 N) through the 18G syringe needle, which corresponded well with the previous literature.[37] Incorporation of PCL nanoparticles slightly increased injection force, but it was still in an easily extruded range (2.34±0.24 N for 7STH50-PCL made by LNP formulation). Since the larger PCL nanoparticles were beneficial to stably release biomolecules for a longer period and the incorporation of these relatively large-sized PCL nanoparticles did not impede injectability, we defined PCL nanoparticles made by LNP formulation as an optimized drug carrier type. PCL nanoparticles prepared by the LNP formulation were used for all the following experiments and hereafter PCL nanoparticles refer to those formulated by the LNP method only.

To assess mechanical stability, compression tests were conducted on STH with different silicate amounts and with or without PCL nanoparticles. The results indicated that storage modulus of the STH was increased with higher silicate amount and the incorporation of PCL nanoparticles (Fig. 3c). We also conducted strain sweep rheology experiments to examine the linear viscoelastic range of PCL nanoparticles-incorporated STHs. The strain was varied from 0.1% to 1000%, while the frequency and temperature were constantly held at 1 Hz and 37 °C. As shown in Fig. 3d, at the low strain condition, moduli of STHs was independent of the strain amplitude and showed linear viscoelastic behavior. However, beyond the critical strain point, the moduli of STHs rapidly decreased, as their internal structure was disturbed. Overall storage moduli of STHs were increased when PCL nanoparticles were included.

When the total solid weight percent in STH was increased from 6 wt% to 7 wt%, the stiffness of STH was increased, but the linear viscoelastic ranges were slightly decreased.

Recovery tests of STHs were conducted at 1 Hz by applying oscillatory strain conditions with low (1%) and high (100%) strain amplitudes. After applying high strain beyond the linear viscoelastic range, we monitored recovery of STH during low strain condition. As shown in Fig. 3e, 6STH50 and 7STH50 with and without PCL nanoparticles exhibited instantaneous mechanical recovery within a few seconds, indicating rapid self-healing of physically crosslinked STHs. Taken together, incorporation of PCL nanoparticles in STHs did not impair injectability or shear-thinning behavior of composite materials.

To further confirm stability/degradability of PCL nanoparticles-incorporated STHs under the physiologically relevant condition, we incubated the composite STH materials in cell culture medium at 37 °C and measured the remaining mass at different time points. The degradation profile showed a gradually decreasing weight loss tendency with remaining mass higher than 80 wt% during the first week, as shown in Fig. 3f. After 50 days, mass-loss in 6STH50-PCL and 7STH50-PCL were 41.1±2.1 wt% and 39.6±2.3 wt%, respectively. Since bone regeneration takes several weeks to months, the composite STH material with stable degradation may correspond well with the regeneration rate of skeletal tissue.

3.3. STH with PCL nanoparticles to fill voids and defects of varied geometries

After analyzing mechanical properties and stable degradation of PCL nanoparticles-incorporated STHs, we tested continuous injection of composite STH materials for building 3D structures *via* a customized injecting device that can continuously and simultaneously inject multiple hydrogels through a single extrusion head. Each syringe was independently connected to a pneumatic syringe pump, enabling the injection of hydrogels with varying composition in a continuous manner (Fig. 4a). The two types of hydrogels made from 7STH50-PCL and 6STH50-PCL could be injected by a similar level of pressure (30–40 Pa). As shown in Fig. 4b–c, both types of composite STHs injected by the device could assemble into 3D structures. In addition, two composite STHs could be simultaneously injected through the multineedle/single-head injecting system to form a 3D structure, in a continuous manner (Fig. 4d). Notably, as shown in Fig. 4e, simultaneously injected composite STHs integrated well with each other and were stable enough to maintain its two-layered structure in an aqueous solution. To demonstrate cavity filling capacity of our injectable composite STHs, we prepared various shapes of empty structures in transparent PDMS substrates for easier observation. As shown in Fig. 4f–h, injected composite STHs could completely fill the void space from bottom to top while maintaining its layered structure. In Fig. 4i–j, we also demonstrated that injected composite STHs were useful to fill complex structures with narrow and sharp edges. To further verify that these injectable composite STHs could fill bone defects with any size and shape, we prepared porcine bone from local butcher and generated random-structured defects by using a micro-drilling machine. As shown in Figure 4k–l, extruded composite STHs could completely fill the defect site to give a smooth surface, while maintaining a heterogeneous structure.

3.4. *In vitro* assessment of cell-laden STH with PCL nanoparticles

The cellular viability within the STH with or without PCL nanoparticles is presented in Fig. 5a. By live/dead fluorescent staining, it was observed that the novel biomaterial showed excellent cellular viability, as the vast portion of cells were alive, as shown in green, with just a minute portion of dead cells, stained in red. The cell viability was determined at day 7 for mouse endothelial cells (EC) in monoculture (86.6±9.5), EC in monoculture with addition of PCL nanoparticles (80±11.3), co-culture with mouse endothelial cells and osteoblasts (EC and OB) (86.1±8.1) or co-culture with EC and OB with the addition of PCL nanoparticles (88±1.5), based on the fluorescence images. This confirms previous demonstrations of biocompatibility of biomaterials composed of gelatine, silicate, or PCL. [56–58] To differentiate between endothelial cells and osteoblasts within the cell-laden gels, cell trackers were employed. Fluorescence imaging shown in Fig. 5b revealed the presence of both live endothelial cells (red) and osteoblasts (green) within the PCL nanoparticle-laden constructs. It was observed that both cell types remained viable, and increased in numbers for up to 21 days of culture. Although the VEGF-releasing STH portion and solely osteogenic STH portion originated from separate reservoirs, they were merged and injected in unison; however, the cells did not migrate out of their initial portions into the other. The proliferation of cells within the biomaterial gel, as assessed by the PrestoBlue test, is presented in Fig. 5c. Cell numbers increased significantly over the course of the 7 days in culture. The presence of VEGF-encapsulated PCL nanoparticles significantly increased (p< 0.05) the proliferation rate of endothelial cells. Furthermore, the presence of osteoblasts significantly increased (p< 0.05) the proliferation rate of endothelial cells. Taken together, these results showed that the osteoblasts did not require direct contact with the endothelial cells to impart enhanced proliferation, and most likely it was caused by paracrine communication signals. Indeed, osteoblast conditioned media has been previously shown to enhance proliferation and sprouting frequency of endothelial cells.[59]

When BMSCs and HUVECs were co-cultured in STH containing VEGF-encapsulated PCL nanoparticles, their osteogenic and angiogenic gene expression profiles were assessed compared to monoculture of either BMSCs or HUVECs (Fig. 5d). Data shows that there was a significant increase in the osteogenic gene expression in the co-culture compared to BMSC alone as evidenced by a significant fold change increase in the expressions of *ALP* and *OC*. Similarly, the presence of BMSCs in co-culture enhanced the angiogenic gene expressions of HUVECs, whereby there was a significant increase in fold change *VCAM* gene expression compared to monoculture of HUVECs. This demonstrated the synergistic relationship of these cell types. Indeed, it was recently shown that BMSCs impart a enhanced angiogenic gene expression by HUVECs, while HUVECs improved the osteogenic markers expression in BMSC.[60] We demonstrate in the current study that this enhanced differentiation achieved by co-culture is attainable in this novel STH gel with VEGF-encapsulated PCL nanoparticles, even when BMSCs and HUVECs portions were injected from separate gel reservoirs and merged into one dual-layer hydrogel. However, although STH significantly enhanced the growth and activity of the osteogenic cells and endothelial cells *in vitro*, our study has the limitation that endothelial cells did not form a highly connective blood vessel structure and *in vivo* bone formation analysis was not conducted. In this respect, an interesting future study will be the formation of perfusable

blood vessel structures in an injectable STH and evaluation of its anastomosis with native blood vessels *in vivo*, to improve bone tissue regeneration.

4. Conclusions

In this introductory study, we have defined the optimal composition of an injectable STH to deliver cells and growth factors in a layered structure, and conducted initial cell characterization studies. We used osteogenic silicate-based STHs for the base material and incorporated VEGF-releasing PCL nanoparticles as a growth factor carrier in the endothelial cell encapsulated hydrogel, which was composed of softer STHs. Furthermore, the negatively charged PCL nanoparticles did not alter the shear thinning behaviour of the STH. Subsequently, these STHs could be simultaneously injected and the extruded STHs could fill defects of various geometries while maintaining their dual structures in a continuous manner. From *in vitro* testing, we demonstrated that osteogenic cells and endothelial cells co-cultured in the extruded pattered composite hydrogel showed enhanced growth compared to cells cultured in monoculture. We expect this novel platform will be the first step of developing an injectable scaffold for providing a stable matrix that completely fills the irregularly shaped bone defects and supports the formation of continuous blood vessel network throughout the regenerating bone tissue.

Acknowledgments

References

1. Einhorn TA, Gerstenfeld LC. Nat Rev Rheumatol. 2015; 11:45–54. [PubMed: 25266456]

2. Kumar S, Wan C, Ramaswamy G, Clemens TL, Ponnazhagan S. Mol Ther. 2010; 18:1026–1034. [PubMed: 20068549]

3. Fong K, Truong V, Foote CJ, Petrisor B, Williams D, Ristevski B, Sprague S, Bhandari M. BMC Musculoskeletal Disord. 2013; 14:103.

4. Heckman JD, Sarasohn-Kahn J. Bull Hosp Jt Dis. 1997; 56:63–72. [PubMed: 9063607]

5. Green DP. J Hand Surg Am. 1985; 10:597–605. [PubMed: 3900189]

6. Lafforgue P. Jt, Bone, Spine. 2006; 73:500–507.

7. Tomlinson RE, Silva MJ. Bone Res. 2013; 1:311. [PubMed: 26273509]

8. Utvåg SE, Grundnes O, Rindal DB, Reikerås O. J Orthop Trauma. 2003; 17:430–435. [PubMed: 12843728]

9. Marrella A, Lee TY, Lee DH, Karuthedom S, Syla D, Chawla A, Khademhosseini A, Jang HL. Mater Today. 2017; doi: 10.1016/j.mattod.2017.10.005

10. Amini AR, Laurencin CT, Nukavarapu SP. CRC Crit Rev Bioeng. 2012; 40:363–408.

11. Calori GM, Colombo M, Mazza E, Ripamonti C, Mazzola S, Marelli N, Mineo GV. Injury. 2013; 44:S63–S69. [PubMed: 23351875]

12. Rao RR, Stegemann JP. Cytotherapy. 2013; 15:1309–1322. [PubMed: 23999157]

13. Ollivier M, Gay AM, Cerlier A, Lunebourg A, Argenson JN, Parratte S. Injury. 2015; 46:1383–1388. [PubMed: 25933808]

14. Almubarak S, Nethercott H, Freeberg M, Beaudon C, Jha A, Jackson W, Marcucio R, Miclau T, Healy K, Bahney C. Bone. 2016; 83:197–209. [PubMed: 26608518]

15. Mercado-Pagán ÁE, Stahl AM, Shanjani Y, Yang Y. Ann Biomed Eng. 2015; 43:718–729. [PubMed: 25616591]

16. Yu L, Li Y, Zhao K, Tang Y, Cheng Z, Chen J, Zang Y, Wu J, Kong L, Liu S. PLoS One. 2013; 8:e62570. [PubMed: 23638115]

17. Lai PL, Tai CL, Chen LH, Nien NY. BMC Musculoskeletal Disord. 2011; 12:116.

18. Vaishya R, Chauhan M, Vaish A. J Clin Orthop Trauma. 2013; 4:157–163. [PubMed: 26403875]

19. Kusumbe AP, Ramasamy SK, Adams RH. Nature. 2014; 507:323–328. [PubMed: 24646994]

20. Kang Y, Mochizuki N, Khademhosseini A, Fukuda J, Yang Y. Acta Biomater. 2015; 11:449–458. [PubMed: 25263031]

21. Ramasamy SK, Kusumbe AP, Wang L, Adams RH. Nature. 2014; 507:376–380. [PubMed: 24647000]

22. Liu X, Chen W, Zhang C, Thein-Han W, Hu K, Reynolds MA, Bao C, Wang P, Zhao L, Xu HHK. Tissue Eng, Part A. 2017; 23:546–555. [PubMed: 28287922]

23. Li Q, Wang Z. Arch Med Res. 2013; 44:504–513. [PubMed: 24120387]

24. Kazemzadeh-Narbat M, Rouwkema J, Annabi N, Cheng H, Ghaderi M, Cha BH, Aparnathi M, Khalilpour A, Byambaa B, Jabbari E. Adv Healthcare Mater. 2017; 6:1601122.

25. Byambaa B, Annabi N, Yue K, Trujillo-de Santiago G, Alvarez MM, Jia W, Kazemzadeh-Narbat M, Shin SR, Tamayol A, Khademhosseini A. Adv Healthcare Mater. 2017; 6:1700015.

26. Findlay DM, Haynes DR. Mod Rheumatol. 2005; 15:232–240. [PubMed: 17029071]

27. Aharinejad S, Marks SC, Böck P, MacKay CA, Larson EK, Tahamtani A, Mason-Savas A, Firbas W. Anat Rec. 1995; 242:111–122. [PubMed: 7604975]

28. Walsh DA, Mapp PI. Rheumatology. 1998; 37:1032–1033.

29. Taichman RS, Cooper C, Keller ET, Pienta KJ, Taichman NS, McCauley LK. Cancer Res. 2002; 62:1832–1837. [PubMed: 11912162]

30. Gaharwar AK, Mihaila SM, Swami A, Patel A, Sant S, Reis RL, Marques AP, Gomes ME, Khademhosseini A. Adv Mater. 2013; 25:3329–3336. [PubMed: 23670944]

31. Ruzicka B, Zaccarelli E. Soft Matter. 2011; 7:1268–1286.

32. Pawar N, Bohidar H. J Chem Phys. 2009; 131:07B617.

33. Gaharwar AK, Kishore V, Rivera C, Bullock W, Wu CJ, Akkus O, Schmidt G. Macromol Biosci. 2012; 12:779–793. [PubMed: 22517665]

34. Gaharwar AK, Schexnailder P, Kaul V, Akkus O, Zakharov D, Seifert S, Schmidt G. Adv Funct Mater. 2010; 20:429–436.

35. Gaharwar AK, Schexnailder PJ, Kline BP, Schmidt G. Acta Biomater. 2011; 7:568–577. [PubMed: 20854941]

36. Thompson DW, Butterworth JT. J Colloid Interface Sci. 1992; 151:236–243.

37. Avery RK, Albadawi H, Akbari M, Zhang YS, Duggan MJ, Sahani DV, Olsen BD, Khademhosseini A, Oklu R. Sci Transl Med. 2016; 8:365ra156–365ra156.

38. Gaharwar AK, Avery RK, Assmann A, Paul A, McKinley GH, Khademhosseini A, Olsen BD. ACS Nano. 2014; 8:9833–9842. [PubMed: 25221894]

39. Yang YQ, Tan YY, Wong R, Wenden A, Zhang LK, Rabie ABM. In J Oral Sci. 2012; 4:64–68.

40. Street J, Bao M, deGuzman L, Bunting S, Peale FV, Ferrara N, Steinmetz H, Hoeffel J, Cleland JL, Daugherty A, van Bruggen N, Redmond HP, Carano RAD, Filvaroff EH. Proc Natl Acad Sci U S A. 2002; 99:9656–9661. [PubMed: 12118119]

41. Kumar N, Chaurasia S, Patel RR, Khan G, Kumar V, Mishra B. RSC Adv. 2016; 6:16520–16532.

42. Sipahigil O, Alarçin E, Türkoğlu M, Dortunç B, Karagöz H, Ülkür E, Vural İ, Çapan Y. Nobel Med. 2012; 8:77–82.

43. Rui J, Dadsetan M, Runge MB, Spinner RJ, Yaszemski MJ, Windebank AJ, Wang H. Acta Biomater. 2012; 8:511–518. [PubMed: 22019759]

44. d'Angelo I, Oliviero O, Ungaro F, Quaglia F, Netti PA. Acta Biomater. 2013; 9:7389–7398. [PubMed: 23523534]

45. Liu W, Zhang YS, Heinrich MA, De Ferrari F, Jang HL, Bakht SM, Alvarez MM, Yang J, Li YC, Trujillode Santiago G. Adv Mater. 2016

46. Santhosh KT, Alizadeh A, Karimi-Abdolrezaee S. J Controlled Release. 2017; 261:147–162.

47. Shubhra QTH, Kardos AF, Feczkó T, Mackova H, Horák D, Tóth J, Dósa G, Gyenis J. J Microencapsulation. 2014; 31:147–155. [PubMed: 23875616]

48. Pieper S, Langer K. Mater Today: Proceedings. 2017; 4:S188–S192.

49. Mittal G, Sahana DK, Bhardwaj V, Kumar MNVR. J Controlled Release. 2007; 119:77–85.

50. Zakeri-Milani P, Loveymi BD, Jelvehgari M, Valizadeh H. Colloids Surf, B. 2013; 103:174–181.

51. Rafiei P, Haddadi A. Int J Nanomed. 2017; 12:935–947.

52. Lee TY, Ku M, Kim B, Lee S, Yang J, Kim SH. Small. 2017

53. Park JY, Shim JH, Choi SA, Jang J, Kim M, Lee SH, Cho DW. J Mater Chem B. 2015; 3:5415–5425.

54. Kempen DHR, Lu L, Heijink A, Hefferan TE, Creemers LB, Maran A, Yaszemski MJ, Dhert WJA. Biomaterials. 2009; 30:2816–2825. [PubMed: 19232714]

55. Mu L, Feng SS. J Controlled Release. 2003; 86:33–48.

56. Brennan MÁ, Renaud A, Gamblin A-l, D'Arros C, Nedellec S, Trichet V, Layrolle P. Biomed Mater. 2015; 10:045019. [PubMed: 26238732]

57. Nair BP, Sindhu M, Nair PD. Colloids Surf, B. 2016; 143:423–430.

58. Zou Y, Taheri Qazvini N, Zane K, Sadati MS, Wei Q, Liao J, Fan J, Song D, Liu J, Ma C. ACS Appl Mater Interfaces. 2017; 9:15922–15932. [PubMed: 28406027]

59. Liu C, Cui X, Ackermann TM, Flamini V, Chen W, Castillo AB. Integr Biol. 2016; 8:785–794.

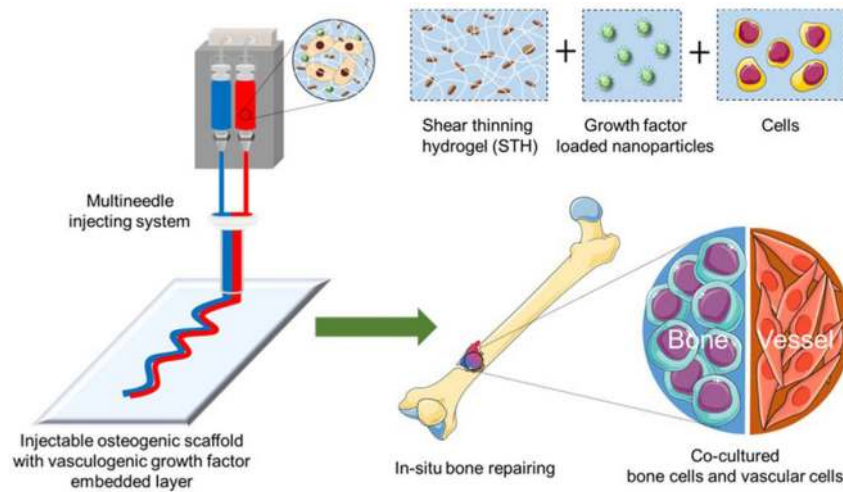60. Böhrnsen F, Schliephake H. Int J Oral Sci. 2016; 8:223–230. [PubMed: 27910940]

Fig. 1.

A schematic illustration showing a dual-layer structure of STH that can be injected through a customized multineedle injecting device. Osteogenic hydrogels consist of silicate nanoplatelet-based STH that encapsulates osteogenic cells. STH can also incorporate VEGF-loaded PCL nanoparticles to deliver endothelial cells. Injected hydrogel structure can fill the bone defect of any shape and size.
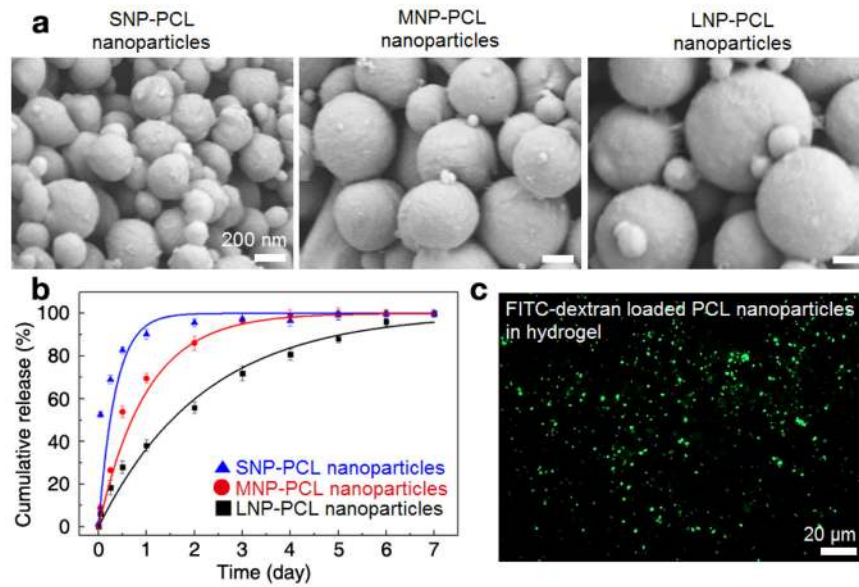
Fig. 2.
Biodegradable PCL nanoparticles that can store and release growth factors in STH. a) FESEM images of the synthesized PCL nanoparticles with various particle sizes, which were prepared by different formulation codes (SNP for small-sized nanoparticles, MNP for medium-sized nanoparticles, and LNP for large-sized nanoparticles). b) Cumulative release of the FITC-dextran molecules from the PCL nanoparticles with different diameters of 268±11 nm (SNP, blue triangle), 429 ±17 nm (MNP, red circle) and 743±37 nm (LNP, black square). Fluorescence level of the supernatant of the PCL nanoparticles incubated in PBS was measured by a microplate reader. The error bar represents the standard deviation of the three times experiments. c) The fluorescence microscope image showing a homogeneous dispersion of FITC-dextran encapsulated PCL nanoparticles in silicate-based STH.
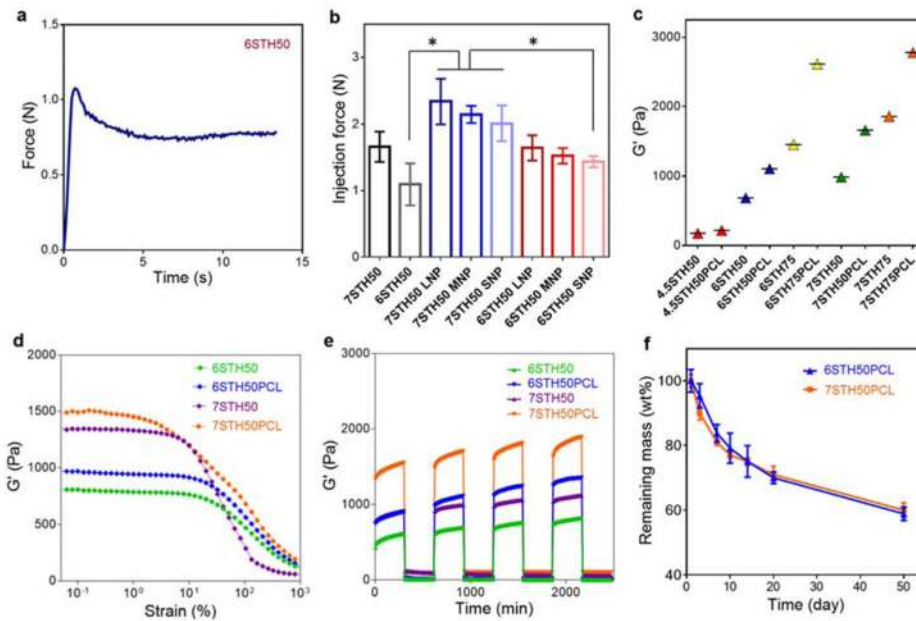
Fig. 3.
Injectability, storage modulus, shear thinning property, and degradability of PCL nanoparticles-incorporated STH. a) The required injection force of STH (6STH50) to pass through needle was measured using an Instron mechanical tester and 3ml syringe with 18 gauge needle, at a constant rate of 2 mL/min. b) Injection force measurement of PCL nanoparticles-incorporated STH with different preparation formulations was conducted by using an Instron mechanical tester. c) Storage modulus of STHs as a function of nanosilicate amount, solid fraction and PCL nanoparticles. The modulus of elasticity was enhanced by increasing amount of nanosilicate content, solid fraction and the presence of PCL nanoparticles. d) Strain sweep rheology experiments indicated that the linear viscoelastic range decreases with increasing weight percentage of solid weight and PCL nanoparticles in STH. e) Recovery of STHs with and without PCL nanoparticles was monitored by measuring storage moduli and altering high (100%) and low (1%) stain conditions. f) Degradability test of STH in cell culture medium at 37 °C (n=3).
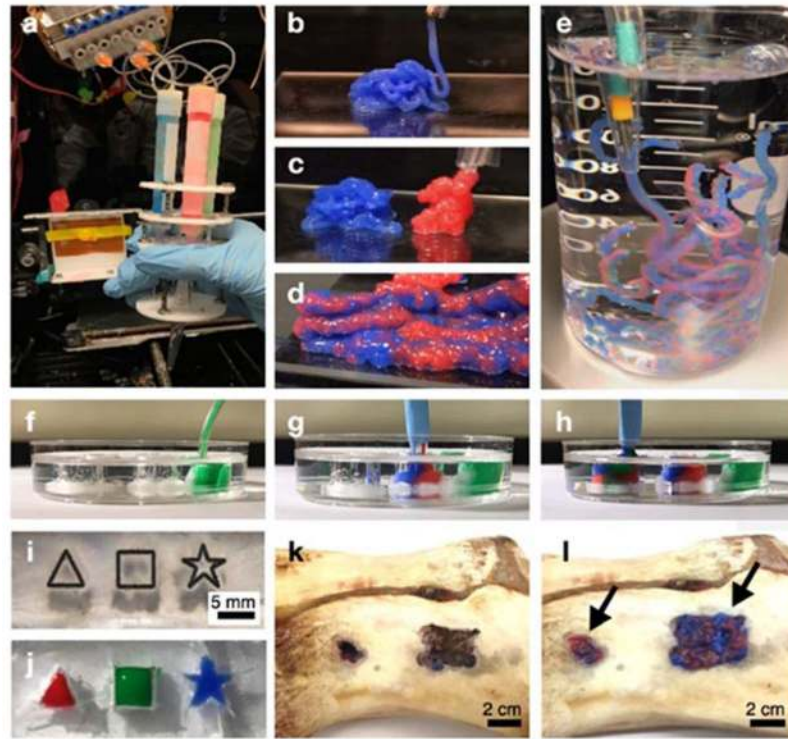
Fig. 4.
Photo images of 3D PCL-incorporated STH structures injected by a multineedle injecting system. a) A customized multineedle injecting device that can continuously and simultaneously inject multiple hydrogel types through the single head system. Each hydrogel syringe can be independently actuated by a separate pump. b–d) Stiffer hydrogels to deliver osteogenic cells (7STH50+PCL, blue) and softer hydrogels to deliver endothelial cells (6STH50+PCL, red) could be injected from the 3D injecting device without physical clogging, in both individual (b, c) and simultaneous (d) modes. e) Injected PCL incorporated STHs were sufficiently stable to maintain their dual-layer structures in an aqueous system. f–j) PCL-incorporated STHs could completely fill the complex empty spaces, including triangle, square, and star shaped void structures that were formed in transparent PDMS substrates. k–l) By using a porcine bone, we demonstrated that our injectable bone implant material could fill the defect sites of bone with any size and shape. Panels k and l show photo images of defect site in the porcine bone before and after injecting dual-layer structured STH, respectively.
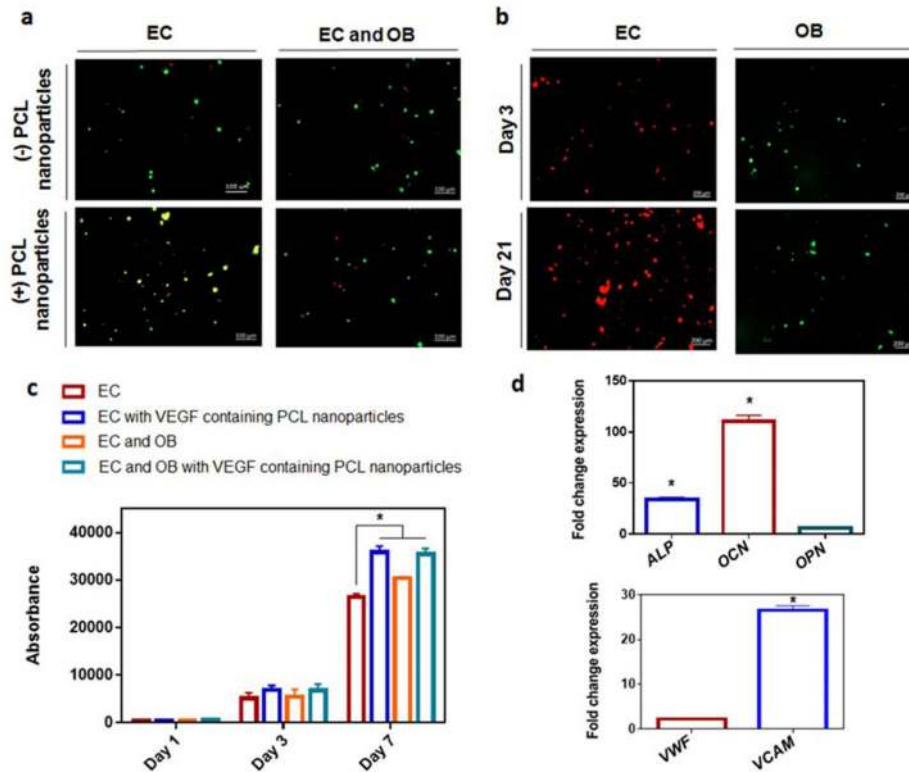
Fig. 5.
Growth and activity of osteogenic cells and vasculogenic cells co-cultured in injected STH material a) Live/dead fluorescent imaging at day 7 of mouse endothelial cells (EC) in monoculture, or co-culture with mouse osteoblasts (EC and OB) with/without the addition of PCL nanoparticles showing live cells in green and dead cells in red. Scale bars represent 100 μm. b) Live cell tracker of EC in red and OB in green cultured for up to 21 days in shear thinning gels with the addition of PCL nanoparticles. Scale bars represent 200 μm. c) Presto blue measurements of monoculture of EC or co-culture with OB, with/without the addition of VEGF-containing PCL nanoparticles to the STH. d) Gene expression within STH with VEGF-containing PCL nanoparticles. Fold change gene expression of co-cultures of BMSCs with HUVECs cells in, relative to monoculture of either BMSCs (for osteogenic genes) or HUVECs (for angiogenic genes). * indicates statistical differences between indicated groups ($p < 0.05$)

Table 1

Influence of formulation variables on the mean nanoparticle size, and zeta potential of FITC-Dextran-loaded PCL nanoparticles

Formulation code		SNP	MNP	LNP
Experimental conditions ofprimary emulsion process	Amount of PVA solution (2%) in the inner aqueous phase (mL)	10		
	PCL amount (mg)	250		
	Amount of organic solvent (mL)	5		
	Amplitude (%)	50	40	30
	Exposure time (min)	5	3	1
Experimental conditions of double emulsion process	Amount of PVA solution (0.1%) in the outer aqueous phase (mL)	30		
	Amplitude (%)	50	40	30
	Exposure time (min)	5	3	1
Synthesized nanoparticles	Mean particle size (± SD, nm)	268±11	429±17	743±37
	Zeta potential (± SD, mV)	−22.40±0.22	−21.83±0.26	−22.6±0.5

Table 2

List of primer sequences

Genes	Sequences (5′-3′)
GAPDH	F: ACAGTTGCCATGTAGACC
	R: TTTTTGGTTGAGCACAGG
ALP	F: GAGTATGAGAGTGACGAGAA
	R: AGTGGGAGTGCTTGTATC
OPN	F: TTCCAAGTAAGTCCAACGAAAG
	R: GTGACCAGTTCATCAGATTCAT
OCN	F: ATGAGAGCCCTCACACTCCTCG
	R: GTCAGCCAACTCGTCACAGTCC
VWF	F: CCTTGGTCACATCTTCACATTCAC
	R: CTCATCCAGATCCCACACAGA
VCAM	F: ACACTTTATGTCAATGTTGCC
	R: TTGTAGAAATTAAGGTGAGAGTTG